the use of laboratory animals. Briefly, monkeys were anaesthetized with sufentanil citrate (6–12 $\mu g\,kg^{-1}\,h^{-1}$; intravenous (i.v.) injection) and paralysed with Pavulon (pancuronium bromide; 0.05 $mg\,kg^{-1}\,h^{-1}$; i.v.). CO_2 and body temperature were maintained at 4.0% and 37.5 °C, respectively. Each eye was brought into focus on the screen of a Trinitron monitor using custom-fit contact lenses. On two animals with apparent binocular divergence, the two eyes were brought into convergence by a prism. The whole screen occupied a visual field of 19° × 14° that covered the visual field of the recorded portions of V2 (2–7° along the vertical meridian). In one animal, anatomical tracers were injected into V2. Its post-mortem occipital operculum was sectioned in the tangential plane and stained for cytochrome oxidase and tracers. A detailed description of these methods has been published previously[3].

Optical recording

The intrinsic optical signal was recorded using a slow-scan CCD (charge-coupled device) array camera (Photometrics, CH 250 0206) that was focused 0–300 μm below the surface by a tandem lens system. The cortical surface was illuminated by light at 630 ± 15 nm wavelength. In each series of frames, four 103-ms-long frames taken 1.3–2.8 s after the onset of each stimulus were used as response frames. Two background frames were taken at 0.7 and 0.2 s before stimulus onset. Each stimulus, viewed binocularly by the animal, lasted for 3 s and was separated by 10 s of uniform grey on the screen. In each trial, 50 repetitions of each stimulation condition were interlaced pseudo-randomly with other conditions, and the corresponding frames were averaged. A differential image between two stimulation conditions was calculated by subtracting the response frame of one condition from that of the other condition, divided by the first background frame. A single-condition image of one stimulation condition was calculated by dividing the corresponding response frame with the first background frame. For each stimulation condition, a control image was calculated by dividing the second background frame with the first background one. In each trial, four control images derived from four different stimulation conditions were used for the statistical analysis. In each functional image, a pair of gaussian spatial filters (s.d. = 49 and 326 μm, respectively) was used to remove the high and low spatial frequency noises. The four single-condition images corresponding to four different time points under the same stimulation condition were then averaged to obtain the final single-condition image for each condition. For each pixel, the intensity values in these four single-condition images were compared with those in the four control images by the Student's *t*-test, to determine the significance level of the activation. In two animals, a series of frames was taken when the screen was kept at a constant uniform grey (blank presentation). The blank presentations were pseudo-randomly interlaced with the stimulus presentations. When the single-condition images during the blank presentations were used as controls, the regions significantly activated by each stimulus were largely the same as those derived from the above analysis, which used the second background images as controls (Supplementary Fig. 3).

To identify the colour-preferring modules, we used isoluminant red/green gratings (sinusoidal, 0.25 cycles $degree^{-1}$, drifted at 1 cycle s^{-1}), high-contrast achromatic gratings (sinusoidal, 2.0 cycles $degree^{-1}$, 2.0 cycles s^{-1}, 100% luminance contrast) and low-contrast achromatic gratings (sinusoidal, 0.25 cycles $degree^{-1}$, 2.5 cycles s^{-1}, 7% luminance contrast). They all had an average luminance of 10 $cd\,m^{-2}$ and four orientations (0°, 90°, 45° and 135°). The two colours in the red/green gratings corresponded to the colours of the red and green phosphors of the cathode-ray tube, respectively (see Fig. 1a). The colour-preferring modules that we identified appeared dark in the differential image that subtracted the responses to high-contrast achromatic gratings from those to isoluminant gratings, but not in the differential image that subtracted the responses to high-contrast gratings from those to low-contrast achromatic gratings.

To study the cortical activation evoked by a single colour, we used static, colour/grey gratings (square wave, 0.25 cycles $degree^{-1}$, two alternating spatial phases, 0°, 90°, 45°, 135°), or uniform colours covering the full screen (10 $cd\,m^{-2}$). CIE-*xy* chromaticity coordinates of the tested colours are: red (0.55, 0.33), orange (0.54, 0.40), yellow (0.45, 0.47), lime (0.35, 0.54), green (0.27, 0.49), aqua (0.23, 0.36), blue (0.16, 0.08), purple (0.23, 0.11), pink (0.38, 0.27), and white and grey (0.31, 0.31). The uniform grey between stimuli and the grey in each grating had a luminance of 10 $cd\,m^{-2}$. In isoluminant gratings, all colours had a luminance of 10 $cd\,m^{-2}$. In luminance-varying gratings, the luminance of different colours were (in $cd\,m^{-2}$): red, 14; orange, 18; yellow, 28; green, 19; aqua, 22; blue, 8; purple, 11. These values are similar to those used by ref. 9 so that they reflect the difference in luminance of the colours described by different names of a natural language.

Electrode recording

Electrode penetrations were made vertically with the guide of functional maps. All units were recorded between 0 and 1 mm below cortical surfaces. After the receptive field of a single- or multi-unit was plotted, flashed colour bars or drifting colour/grey gratings (1.5 cycles $degree^{-1}$, 1 cycle s^{-1}) were presented in the receptive field for 1.28 s every 3.28 s. Net neuronal responses were obtained by subtracting the spontaneous firing rate during 1 s before the presentation of each stimulus from that during the presentation. Ten repetitions of each stimulus were interlaced pseudo-randomly with other stimuli, and their net neuronal responses were averaged to obtain the mean response to the stimulus.

Received 30 September; accepted 26 November 2002; doi:10.1038/nature01372.

1. Komatsu, H. Mechanisms of central colour vision. *Curr. Opin. Neurobiol.* **8,** 503–508 (1998).
2. Ts'o, D. Y., Roe, A. W. & Gilbert, C. D. A hierarchy of the functional organization for colour, form and disparity in primate visual area V2. *Vision Res.* **41,** 1333–1349 (2001).
3. Xiao, Y., Zych, A. & Felleman, D. J. Segregation and convergence of functionally defined V2 thin stripe and interstripe compartment projections to area V4 of macaques. *Cereb. Cortex* **9,** 792–804 (1999).
4. Roe, A. W. & Ts'o, D. Y. Visual topography in primate V2: Multiple representation across functional stripes. *J. Neurosci.* **15,** 3689–3715 (1995).
5. Malonek, D. & Grinvald, A. Interactions between electrical activity and cortical microcirculation revealed by imaging spectroscopy: Implications for functional brain mapping. *Science* **272,** 551–554 (1996).
6. Tootell, R. B. & Hamilton, S. L. Functional anatomy of the second visual area (V2) in the macaque. *J. Neurosci.* **9,** 2620–2644 (1989).
7. Burkhalter, A. & Van Essen, D. C. Processing of colour, form and disparity information in visual areas VP and V2 of ventral extrastriate cortex in the macaque monkey. *J. Neurosci.* **6,** 2327–2351 (1986).
8. Levitt, J. B., Kiper, D. C. & Movshon, J. A. Receptive fields and functional architecture of macaque V2. *J. Neurophysiol.* **71,** 2517–2542 (1994).
9. Yoshioka, T., Dow, B. M. & Vautin, R. G. Neuronal mechanisms of colour categorization in areas V1, V2 and V4 of macaque monkey visual cortex. *Behav. Brain Res.* **76,** 51–70 (1996).
10. Hubel, D. H. & Livingstone, M. S. Segregation of form, colour, and stereopsis in primate area 18. *J. Neurosci.* **7,** 3378–3415 (1987).
11. DeYoe, E. A. & Van Essen, D. C. Segregation of efferent connections and receptive field properties in visual area V2 of the macaque. *Nature* **317,** 58–61 (1985).
12. Peterhans, E. & von der Heydt, R. Functional organization of area V2 in the alert macaque. *Eur. J. Neurosci.* **5,** 509–524 (1993).
13. Gegenfurtner, K. R., Kiper, D. C. & Fenstemaker, S. B. Processing of colour, form, and motion in macaque area V2. *Vis. Neurosci.* **13,** 161–172 (1996).
14. Kiper, D. C., Fenstemaker, S. B. & Gegenfurtner, K. R. Chromatic properties of neurons in macaque area V2. *Vis. Neurosci.* **14,** 1061–1072 (1997).
15. Moutoussis, K. & Zeki, S. Responses of spectrally selective cells in macaque area V2 to wavelengths and colors. *J. Neurophysiol.* **87,** 2104–2112 (2002).

Supplementary Information accompanies the paper on *Nature*'s website (http://www.nature.com/nature).

Acknowledgements We thank L. Cleary, E. Kaplan, J. Maunsell and J. Krauskopf for their suggestions on the manuscript. We also thank A. Zych and X. Huang for computer programming, Q. Huang for technical support and J. Chen for discussion. This research was supported by an individual grant from the National Eye Institute to D.J.F. and a core grant from the National Eye Institute to the University of Texas, Health Science Center at Houston.

Competing interests statement The authors declare that they have no competing financial interests.

Correspondence and requests for materials should be addressed to Y.X. (e-mail: youping@camelot.mssm.edu).

Inhibitory feedback required for network oscillatory responses to communication but not prey stimuli

Brent Doiron*†, Maurice J. Chacron*†, Leonard Maler†, André Longtin* & Joseph Bastian‡

** Physics Department, University of Ottawa, Ottawa, Ontario K1N 6N5, Canada*
† Department of Cellular and Molecular Medicine, University of Ottawa, Ottawa, Ontario K1H 8M5, Canada
‡ Department of Zoology, University of Oklahoma, Norman, Oklahoma 73019, USA

Stimulus-induced oscillations occur in visual[1,2], olfactory[3–6] and somatosensory[7] systems. Several experimental[2,3,5] and theoretical[8–13] studies have shown how such oscillations can be generated by inhibitory connections between neurons. But the effects of realistic spatiotemporal sensory input on oscillatory network dynamics and the overall functional roles of such oscillations in sensory processing are poorly understood. Weakly electric fish must detect electric field modulations produced by both prey (spatially localized)[14] and communication (spatially diffuse)[15] signals. Here we show, through *in vivo* recordings, that sensory pyramidal neurons in these animals produce an oscillatory response to communication-like stimuli, but not to prey-like stimuli. On the basis of well-characterized circuitry[16], we construct a network model of pyramidal neurons that predicts that diffuse delayed inhibitory feedback is required to achieve oscil-

latory behaviour only in response to communication-like stimuli. This prediction is experimentally verified by reversible blockade of feedback inhibition that removes oscillatory behaviour in the presence of communication-like stimuli. Our results show that a sensory system can use inhibitory feedback as a mechanism to 'toggle' between oscillatory and non-oscillatory firing states, each associated with a naturalistic stimulus.

Organisms must discriminate between sensory inputs with varying spatiotemporal structure. Electric fish offer a clear example because prey and communication signals differ greatly in their spatial extent. Sensory systems have evolved architectures to process such signals efficiently. Feedback connections are common in neural systems, especially at the thalamo-cortical level, where they control sensory transmission[2]. Feedback is also a prominent feature of brainstem electrosensory circuitry, and its organization parallels that of cortico-thalamic pathways[16]. We show here how inhibitory feedback allows electrosensory lateral line lobe (ELL) pyramidal neurons[16] to switch between non-oscillatory and oscillatory states, each associated with prey-like or communication-like stimuli, respectively.

The electric fish *Apteronotus leptorhynchus* produces an electric field through a rhythmic electric organ discharge (EOD). Electroreceptors respond to amplitude modulations of this field produced by conspecifics or objects. These afferents encode amplitude modulations[17] and synapse onto ELL pyramidal neurons[16,18]. Two stimulus geometries, 'local' and 'global', were used to activate receptor afferents and pyramidal neurons (see Methods). Local geometry applies the stimulus to a small fraction of the fish's skin, stimulating only a portion of the centre of the receptive field of a pyramidal neuron from which we record (Fig. 1a, left). This produces localized amplitude modulations of the fish's own EOD that are spatially similar to those produced by small aquatic invertebrate prey[14]. Global geometry, however, applies a bilateral stimulus homogenously to the whole fish, stimulating both the centre and surround receptive fields of pyramidal neurons (Fig. 1b, left). This produces amplitude modulations that are spatially similar to communication signals[15]. Large objects (obstacles, root masses) will produce spatially extensive amplitude modulations, but these are expected to be heterogeneous. These fish routinely give communication responses[15] in response to global stimuli with gaussian temporal structure (data not shown), showing that these effectively mimic communication stimuli.

Figure 1 shows a typical pyramidal cell response recorded *in vivo* when band-limited gaussian EOD amplitude modulations (0–40 Hz) were applied locally or globally ($n = 15$). With local stimulation, the spike time autocorrelation[19], $A(\tau)$, was positive at small values of the lag, τ (after a negative correlation owing to refractoriness), and histograms of the interspike interval (ISI) showed a single peak (Fig. 1a, middle and right). $A(\tau)$ shows that the spikes are not independent of each other; rather, there is a tendency to produce high-frequency (~100-Hz) clusters of spikes[20]. By contrast, when the stimulus was applied globally, a damped oscillation in $A(\tau)$ and two distinct peaks in the ISI histogram appeared, suggesting oscillatory (and/or bursting) behaviour (Fig. 1b, middle and right); no such structure is observed for local stimulation. It is this transition from non-oscillatory to oscillatory behaviour contingent on the switch from local to global stimulation that is the focus of our study.

To verify the presence of oscillatory behaviour and to compare quantitatively the discharge patterns under both stimulus geometries, we computed the power spectral densities (PSDs) of the spike train during both global and local stimulation (Fig. 1d). There was a significant peak in the PSDs during global stimulation (32.41 ± 3.92 Hz; $n = 15$) that was absent during local stimulation, demonstrating that the spike train is oscillatory only during global stimulation. Using the PSDs, we defined an 'oscillation index' (see Methods); this index was larger under global (10.12 ± 3.68 spikes^2 s^{-1}) than under local (2.28 ± 0.62 spikes^2 s^{-1}) geometries (pair-wise t-test, $P = 0.0034$; $n = 15$). In addition, joint interval histograms computed from responses to global and local stimuli differed markedly. Under local stimulation, the joint interval histograms showed no clear structure; however, with global stimuli, short ISIs (<15 ms) were followed preferentially by long ISIs (>15 ms) and vice versa (Fig. 1c). Oscillatory discharge was not observed with local stimulation, even with a contrast up to six times that of the global stimulus, although the peak firing rates were similar to those during global stimulation. These results show that an oscillatory discharge occurs for global but not local stimulation.

The requirement of a global stimulus for oscillatory discharge suggests that the mechanism involves the integration of spatially diffuse inputs. The negative component of $A(\tau)$ at $\tau \approx 15$ ms suggests that delayed inhibitory processes are also involved. ELL circuitry is well described and indicates that feedforward pathways satisfying these criteria are unlikely to exist[16]. But ELL pyramidal neurons project to an isthmic structure (n. praeminentialis dorsalis), which in turn provides several feedback projections to the ELL[16]. This includes a spatially diffuse delayed (~15 ms) inhibitory pathway emanating from a small group of bipolar cells that terminates exclusively on ELL pyramidal cells[21–23]. Theoretical analysis of models of biological and chemical systems with delayed negative feedback have shown how delays can often support oscillatory dynamics[24]; however, little is known about how the spatial extent of a driving stimulus can regulate a feedback-mediated oscillation. Thus, we constructed a neural network model of the ELL to test the hypothesis that delayed inhibitory feedback is sufficient for global stimulus-induced oscillations.

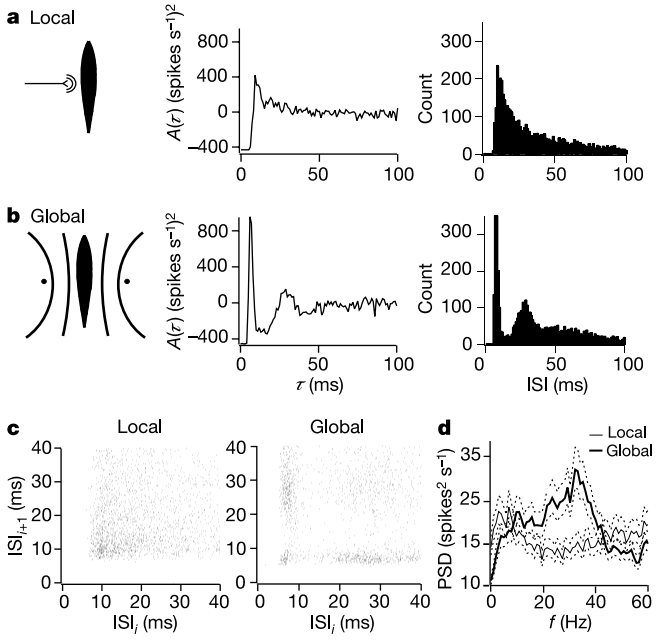

Figure 1 ELL pyramidal neurons show differential responses to local (prey-like) and global (communication-like) stimuli ($n = 15$). **a**, Local stimulation. Left, local stimulus model; a dipole was placed near the skin to stimulate only a part of the pyramidal cell receptive field centre. Middle and right, $A(\tau)$ and ISI histograms of a typical pyramidal cell response to a local stimulus. **b**, Global stimulation. Left, global stimuli model; two $Ag^+/AgCl$ wire electrodes were placed transverse to the fish to produce spatially extensive stimuli. Middle and right, $A(\tau)$ and ISI histograms of pyramidal cell response to a globally applied stimulus. The mean firing rates of the stimulated cell were 21.8 spikes s^{-1} and 22.8 spikes s^{-1} for local and global stimulus geometries, respectively. Note that the same cell was used for both stimuli. **c**, Joint interval histograms under local (left) and global (right) stimulation. **d**, The PSDs of the spike train under local and global stimulus geometries. Broken lines surrounding the PSDs are the 95% confidence bands (±2 s.d.).

In brief, we modelled the pyramidal neurons as a network of leaky integrate-and-fire (LIF) neurons (ref. 19 and see Methods). All neurons transmit their spikes to a central cell population, *G*. For each spike that it receives, *G* feeds back an inhibitory synaptic (α-function[19]) response to all pyramidal neurons in the network after a fixed time delay, τ_d. The physiological interpretation of *G* is the integration of pyramidal cell output by bipolar cells of the n. praeminentialis dorsalis and their GABA (γ-aminobutyric acid)-mediated projection back to the ELL. A diagram of the network model connectivity is shown in the left panel of Fig. 2a.

Each LIF neuron was driven by two sources. The first was a noise input, $\eta_i(t)$, with positive bias (the subscript *i* denotes spatial position), with η being uncorrelated across space. This modelled stochastic spontaneous activity is similar to that seen *in vivo*[20]. The second input source was band-limited (0–40 Hz) gaussian noise, $S(t)$, mimicking the temporal nature of the electrosensory stimulus used in the experiments. To model local geometry, $S(t)$ was applied to a single neuron, whereas global geometry was modelled by applying $S(t)$ homogeneously to all neurons. With local stimulation, $A(\tau)$ and ISI histograms measured from the neuron receiving $S(t)$ were similar to those observed experimentally, indicating a non-oscillatory state (compare Figs 1a and 2a, middle and right). With global stimulation, however, a transition to an oscillatory response was observed, similar to that observed experimentally (compare Figs 1b and 2b, middle and right). The oscillation index of the model was 8.66 spikes^2 s^{-1} during local stimulation and 15.0 spikes^2 s^{-1} during global stimulation. Joint interval histograms constructed from model spike trains during both local and global conditions were qualitatively similar to those constructed from the data.

These model results were insensitive to parameter heterogeneities in the network resulting from the known variability of pyramidal neurons (ref. 20 and see Methods). In addition, a sixfold increase in the contrast of a local stimulus did not induce oscillatory discharge, similar to experimental findings. We have previously proposed a two-compartmental model of ELL pyramidal cells[25] that simulates the single-cell bursting dynamics observed during current injection *in vitro*[26]. We have also qualitatively reproduced the simulation results presented above (Fig. 2) using a network of these more realistic pyramidal cells (see Supplementary Information).

During local stimulation, the only shared input among neurons is from the global inhibitory feedback, *G*. In spite of this common input, the intrinsic noise sources, $\eta_i(t)$, were of sufficient strength to suppress significant correlations between neurons in the network. This is demonstrated in the model network raster plots (Fig. 3a, top), which show a lack of coincident firing between individual neurons during local input, and by network stimulus histograms (summed activity of all neurons) that weakly fluctuate about a constant value (Fig. 3a, middle). The feedback response, *G* (Fig. 3a, bottom), is determined by the network firing pattern, as illustrated by the network spike histograms, and is thus also roughly constant.

During global conditions, however, $S(t)$ was distributed homogeneously over the whole network, evoking stimulus-induced correlations between neurons. This allowed for increased network synchronization, as shown in network raster plots (Fig. 3b, top) and network stimulus histograms (Fig. 3b, middle). As a result of this increased correlation, *G* received near-coincident spikes from across the network, yielding a significant summation of α-function responses. This enhanced response is fed back to all neurons in the network after a delay time, τ_d, causing 'waves' of inhibition that suppress network firing (Fig. 3b, bottom). As an inhibitory wave abates, subsequent stimulus-induced coincident firing across the network develops. Thus, the interplay between stimulus-induced correlations and an associated delayed increase of feedback inhibition creates an oscillation in the network activity with period determined by both the axonal delay, τ_d, and the synaptic time constant α.

The simulation results shown in Figs 2 and 3 suggest that the diffuse delayed inhibitory feedback is an integral component of the pyramidal cell oscillatory response to global stimuli. To verify this experimentally, we used local injection of xylocaine, a sodium channel antagonist, to specifically block the inhibitory feedback component of the tractus stratum fibrosum (StF) pathway ($n = 10$; see Fig. 4 and Methods). The effect of this block was to remove temporarily feedback inhibition to the ELL, effectively opening the loop from the n. praeminentialis dorsalis to ELL. Xylocaine injection reversibly blocked oscillatory responses to globally applied stimuli: $A(\tau)$ showed no damped oscillations and the ISI histograms were unimodal (Fig. 4b, c, black traces). However, these neurons

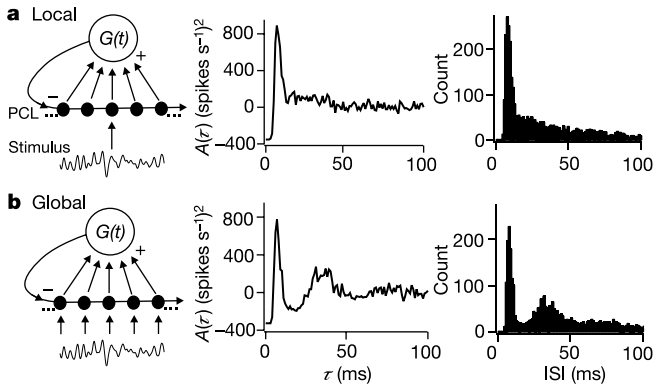

Figure 2 ELL neural network simulations involving global inhibitory feedback show differential responses to local and global stimuli. **a**, Local stimulation. Left, network showing the pyramidal cell layer (PCL) projecting spikes to a kernel, $G(t)$, which feeds back inhibitory responses to the PCL after a delay τ_d. For local stimuli only one cell receives the stimulus (arrow). Middle and right, $A(\tau)$ and ISI histograms of the simulated LIF neuron during local stimulation. **b**, Global stimulation. Left, identical network to that in **a**, but all LIF neurons receive the same stimulus. Middle and right, $A(\tau)$ and ISI histograms of a LIF neuron response to global stimulation. The mean firing rates of the cell were 17.5 spikes s^{-1} and 16.5 spikes s^{-1} for local and global stimulus geometries, respectively.

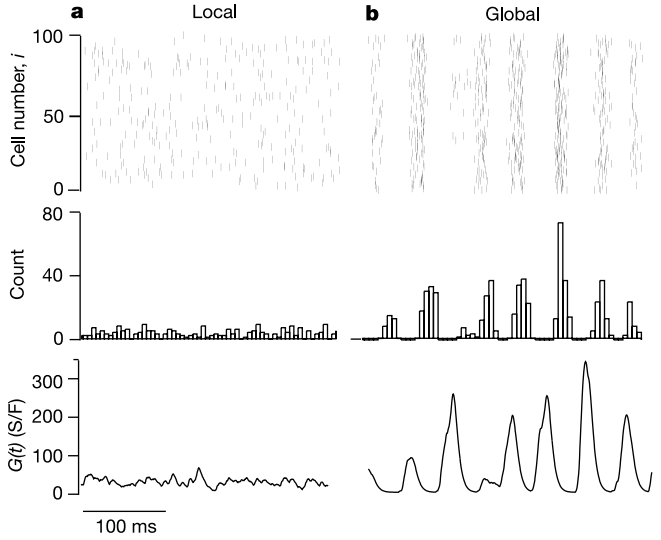

Figure 3 Simulated asynchronous firing and synchronized oscillations during one presentation of a local or global stimulus, respectively. Top, network raster plots under local (**a**) and global (**b**) stimulus with network stimulus histograms shown underneath. Bottom, the total value of the feedback inhibition, $G(t)$, is plotted for the same simulations that gave the spike times.

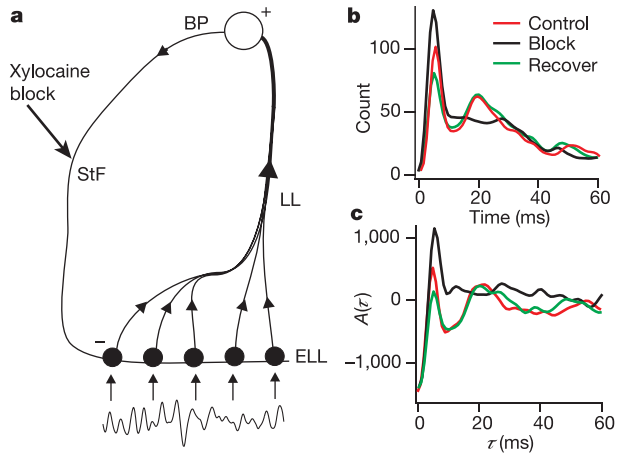

Figure 4 Blockade of the inhibitory component of the StF pathway. **a**, Pyramidal neurons in the ELL project excitatory connections to bipolar cells (BP) of the n. praeminentialis dorsalis through the lateral lemniscus pathway (LL). In turn, the BP cells project back to the ELL through the StF, providing GABA-mediated feedback to the pyramidal neurons. StF axons were blocked by application of xylocaine. **b**, **c**, ISI histograms (**b**) and $A(\tau)$ (**c**) are plotted for control cells (red), during the block (black) and after recovery from xylocaine (green). Histograms and $A(\tau)$ were constructed as in Fig. 1 and smoothed (gaussian-filtered, $\sigma = 5$ ms) to facilitate comparison between states.

showed clear oscillatory behaviour before and after recovery from StF (inhibitory component) blockade (Fig. 4b, c, red traces, control; green traces, recovery). The oscillation indices for control and recovery were similar (pair-wise t-test, $P = 0.353$; $n = 10$) and significantly different from those observed during feedback inhibitory blockade (pair-wise t-test, $P = 0.02$; $n = 10$). These experiments verify the model's prediction that diffuse inhibitory feedback is required for ELL pyramidal neurons to show differential responses to local versus global stimuli.

Our network simulations predict that the synchronization of ELL pyramidal cell firing is an aspect of the oscillatory mechanism involved during global stimulation (Fig. 3). Field potential recordings from the ELL show oscillations during global stimulation (data not shown), consistent with synchronous activity; however, interneuron populations in the ELL[16] and the expected stimulus-driven increase of synchronization during global stimulation complicate the interpretation of this observation.

Inhibition is necessary for synchronization in the olfactory system[3,5] and thalamocortical circuits[2,8]. Modelling studies have shown that synchronous oscillatory solutions exist when inhibitory feedback gain is strong and inhibitory synaptic timescales are long[8,9,11,13], or when there are sufficiently long axonal delays[9,10,13]. Other studies have shown that network oscillations can occur with constant depolarizing input[12] or with increased mean firing rate of uncorrelated excitatory Poisson inputs[13]. In the latter study, oscillations also occurred with increased spatial spread of uncorrelated inputs distributed to the network. In this study, by contrast, synchronous oscillations were produced not by varying feedback gain, intrinsic cellular properties or mean network depolarization, but by simply changing the spatial extent of a stimulus.

It is known that pyramidal neurons can estimate the time course of prey-like stimuli applied under local, but not global, geometries[27]. But these cells do produce bursts of spikes in response to specific features of a global stimulus[28]. These studies suggest that pyramidal cell coding strategies may also depend on the spatial extent of stimuli. We have confirmed that the stimulus encoding abilities of pyramidal cells can be altered during the oscillatory discharge induced by a global stimulus (see Supplementary Information).

We have described a mechanism whereby the spatial extent of stimuli determines the firing behaviour of sensory neurons in the electrosensory system. In addition, these stimuli were spatially similar to those that the fish would encounter in either prey location or communication situations, giving a clear behavioural significance to our results. We have shown that this mechanism requires delayed inhibitory feedback—a very general feature of the nervous system[2,29]. To our knowledge, this is the first demonstration of how delayed inhibitory feedback enables neurons in a sensory channel to toggle between two distinct firing states, with each state connected to a behaviourally relevant stimulus. □

Methods

Physiology

Extracellular single-unit recordings from ELL pyramidal neurons were identified on the basis of recording depth and response patterns[27]. Random amplitude modulations (RAMs) of the EOD were produced by adding an amplitude-modulated sinusoidal waveform to the continuing discharge of the fish. The sinusoid was phase locked to the EOD with a period roughly equal to that of the EOD. RAMs were produced by multiplying the sinusoid by zero-mean band-limited gaussian noise (0–40 Hz, eighth order Butterworth filter). For local geometry, we applied stimuli through a small dipole, tip spacing of 2 mm, positioned at a site in the cell's receptive field centre 2–3 mm lateral to the skin. Global geometry stimuli were applied homogeneously through two electrodes 19 cm lateral to either side of the fish (Fig. 1b, left). The typical global stimulus amplitude was 250 $\mu V\,cm^{-1}$, and the magnitude of the local stimulus was adjusted so that electroreceptor afferent responses were equivalent for either geometry[27]. Histograms and autocorrelation bin widths were 1 ms and were computed from about 4,000 spikes in all cases. ELL pyramidal cells occur in both basilar and non-basilar varieties[18]; our results include both subtypes. We limited recordings to pyramidal neurons from lateral and centrolateral ELL segments with mean spontaneous firing frequencies greater than 15 Hz.

Reversible block of the tractus StF, which conveys descending excitatory and inhibitory inputs to pyramidal neurons[21], was achieved through micropressure ejection of the local anaesthetic xylocaine. A xylocaine filled micropipette (5–10-μm tip diameter) carrying a bipolar pair of 25-μm stainless steel stimulation wires was positioned rostral to the ELL at a depth where electrical stimulation (0.1 ms, 15–25 μA current pulses) evoked the characteristic StF field potential in the ELL[22]. Because the inhibitory component of the StF lies at its ventral-most aspect just dorsal to the lateral lemniscus (ELL efferents)[21], the pipette was positioned just dorsal to a site where antidromic activation of ELL pyramidal neurons occurred. Ejection of xylocaine (2% concentration; 100-ms pulses at 50 p.s.i.) reduced the StF field potential, verifying blockade; the loss of pyramidal cell oscillatory responses paralleled this reduction. Blockade of the dorsal StF, which conveys topographical excitatory feedback[16,22], eliminated the StF field potential but did not prevent global stimulus-induced pyramidal cell oscillations (data not shown). All procedures were in accordance with the University of Oklahoma animal care and use guidelines. The oscillation index was defined as the difference between the maximum and the minimum value of the PSD between 20 and 40 Hz.

Network simulations

We model the ELL pyramidal cell layer as a network of N LIF model neurons[19]. The membrane potential of the ith neuron is labelled $V_i(t)$. When $V_i(t)$ crosses a spike threshold θ, it is reset to the potential (V_{reset}) and a spike is emitted from neuron i. Between spike times ($V_i(t) < \theta$), the dynamics are governed by the following stochastic delay-differential system:

$$\frac{dV_i}{dt} = \frac{-V_i}{\tau_m} + \eta_i(t) + B_i + S_i(t) - G(t-\tau_d)(V_i - V_r) \quad (1)$$

$$G(t) = \frac{g}{N}\sum_{j=1}^{N}\sum_{m=0}^{M_j(t)} \frac{(t-t_{jm})}{\alpha}\exp\left(1-\frac{(t-t_{jm})}{\alpha}\right) \quad (2)$$

τ_m is the passive membrane time constant, and a constant depolarizing bias B_i is set so that, for zero input ($\eta_i = g = S = 0$), each neuron fires periodically ($B_i > \theta/\tau_m$). $\eta_i(t)$ is a zero mean Ornstein–Uhlenbeck process[30], with time constant τ_η. The Ornstein–Uhlenbeck processes are independent ($\eta_i(t)$ and $\eta_j(t)$ are not correlated if $i \neq j$) and the autocorrelation of $\eta_i(t)$ is given by

$$\langle \eta_i(t)\eta_i(t+\tau)\rangle = \frac{\sigma^2}{2\tau_\eta} e^{-\tau/\tau_\eta} \quad (3)$$

RAMs were introduced through a zero mean band-limited (0–40 Hz) gaussian noise, $S(t)$, with variance W. Local stimulation was simulated by applying $S(t)$ to only one LIF neuron, whereas for global stimulus geometry $S(t)$ was applied to all neurons.

The direct inhibitory feedback pathway[16] is modelled by the kernel $G(t)$ in equation (2). $G(t)$ receives spikes from the jth neuron, t_{jm}, over the history of neuron j ($0 \leq m \leq M_j(t)$, where $M_j(t)$ is the total spike count of neuron j at time t). $G(t)$ transforms a spike input, t_{jm}, into an α-function conductance[19] with time constant α. $G(t)$ then projects the summation of all inputs uniformly to all neurons in the network after a fixed delay, τ_d. The gain of the pathway is set by the constant $g > 0$, and $G(t)$ multiplies a battery term ($V_i - V_r$) with reversal potential V_r. The LIF neurons do not have local connections among themselves, as observed for ELL pyramidal cells[16].

The intrinsic model parameters were set to $\tau_m = 10$ ms, $\sigma = 5.5$ nA, $B_i = 0.84$ nA (we

assumed a capacitance of 1 nF) and $\tau_\eta = 15$ ms. These were chosen so that for $S(t) = 0$, $A(\tau)$ and ISI histograms were similar to those observed under spontaneous conditions *in vivo*[20]. We set $N = 100$ to make local and global stimulation significantly distinct. The RAM stimulus variance was $W = 0.238\ \mathrm{nA}^2$, which resulted in firing statistics comparable to those of stimulated pyramidal neurons (Fig. 2). The feedback parameters were set to $g = 390\ \mathrm{S\,F}^{-1}$, $\alpha = 3$ ms, $V_r = V_{reset} = 0$ mV, to model the feedback as $GABA_A$ shunting inhibition, previously reported for interactions between bipolar and pyramidal cells[23]. The loop delay was set to $\tau_d = 12$ ms, allowing a fit to experimental data (Figs 1 and 2), and is also comparable to previously estimated values[22]. Equation (1) was integrated by a simple Euler–Maruyama[30] scheme with $\Delta t = 0.025$ ms. The effects of parameter heterogeneities were tested by choosing B_i and τ_m from gaussian distributions with mean values as given above. The results were qualitatively similar to the homogeneous case for distributions with coefficient of variations of 0.82 and 1.5 for the B_i and τ_m distributions, respectively.

Received 20 August; accepted 26 November 2002; doi:10.1038/nature01360.

1. Gray, C. & Singer, W. Stimulus-specific neuronal oscillations in orientation columns of cat visual cortex. *Proc. Natl Acad. Sci. USA* **86,** 1698–1702 (1989).
2. Sillito, A. M., Jones, H. E., Gerstein, G. L. & West, D. C. Feature-linked synchronization of thalamic relay cell firing induced by feedback from the visual cortex. *Nature* **369,** 479–482 (1994).
3. MacLeod, K. & Laurent, G. Distinct mechanisms for synchronization and temporal patterning of odor-encoding neural assemblies. *Science* **274,** 976–979 (1996).
4. Kashiwadani, H., Sasaki, Y. F., Uchida, N. & Kensaku, M. Synchronized oscillatory discharge of mitral/tufted cells with different molecular receptive ranges in the rabbit olfactory bulb. *J. Neurophysiol.* **82,** 1786–1792 (1999).
5. Stopfer, M., Bhagavan, S., Smith, B. H. & Laurent, G. Impaired odour discrimination on desynchronization of odour-encoding neural assemblies. *Nature* **390,** 70–74 (1997).
6. Friedrich, R. W. & Laurent, G. Dynamic optimization of odor representations by slow temporal patterning of mitral cell activity. *Science* **291,** 889–894 (2001).
7. Ahissar, E. & Vaadia, E. Oscillatory activity of single units in a somatosensory cortex of an awake monkey and their possible role in texture analysis. *Proc. Natl Acad. Sci. USA* **87,** 8935–8939 (1992).
8. Destexhe, A., Contreras, D. & Steriade, M. Mechanisms underlying the synchronization action of corticothalamic feedback through inhibition of thalamic relay cells. *J. Neurophysiol.* **79,** 999–1016 (1998).
9. Bressloff, P. C. & Coombes, S. Dynamics of strongly coupled spiking neurons. *Neural Comput.* **12,** 91–129 (2000).
10. Ernst, U., Pawelzik, K. & Geisel, T. Synchronization induced by temporal delays in pulse-coupled oscillators. *Phys. Rev. Lett.* **74,** 1570–1573 (1995).
11. Wang, X.-J. & Rinzel, J. Spindle rhythmicity in the reticularis thalami nucleus: synchronization among mutually inhibitory neurons. *Neuroscience* **53,** 899–904 (1993).
12. van Vreeswijk, C. & Hansel, D. Patterns of synchrony in neural networks with spike adaptation. *Neural Comput.* **13,** 959–992 (2001).
13. Paulis, Q., Baker, N. B. & Olivier, E. Emergent oscillations in a realistic network: the role of inhibition and the effect of the spatiotemporal distribution of input. *J. Comput. Neurosci.* **6,** 27–48 (1999).
14. Nelson, M. E. & MacIver, M. A. Prey capture in the weakly electric fish *Apteronotus leptorhynchus*: sensory acquisition strategies and electrosensory consequences. *J. Exp. Biol.* **202,** 1195–1203 (1999).
15. Metzner, W. Neural circuitry for communication and jamming avoidance in gymnotiform electric fish. *J. Exp. Biol.* **202,** 1365–1375 (1999).
16. Berman, N. J. & Maler, L. Neural architecture of the electrosensory lateral line lobe: adaptations for coincidence detection, a sensory searchlight and frequency-dependent adaptive filtering. *J. Exp. Biol.* **202,** 1243–1253 (1999).
17. Wessel, R., Koch, C. & Gabbiani, F. Coding of time-varying electric field amplitude modulations in a wave-type electric fish. *J. Neurophysiol.* **75,** 2280–2293 (1996).
18. Maler, L., Sas, E. K. & Rogers, J. The cytology of the posterior lateral line lobe of high frequency weakly electric fish (Gymnotoidei): differentiation and synaptic specificity in a simple cortex. *J. Comp. Neurol.* **195,** 87–139 (1981).
19. Dayan, P. & Abbott, L. F. *Theoretical Neuroscience* (MIT Press, Cambridge, Massachusetts, 2001).
20. Bastian, J. & Nguyenkim, J. Dendritic modulation of burst-like firing in sensory neurons. *J. Neurophysiol.* **85,** 10–22 (2001).
21. Maler, L. & Mugnaini, E. Correlating γ-aminobutyric acidergic circuits and sensory function in the electrosensory lateral line lobe of a gymnotiform fish. *J. Comp. Neurol.* **345,** 224–252 (1994).
22. Berman, N. J., Plant, J., Turner, R. & Maler, L. Excitatory amino acid transmission at a feedback pathway in the electrosensory system. *J. Neurophysiol.* **78,** 1869–1881 (1997).
23. Berman, N. J. & Maler, L. Interaction of $GABA_B$-mediated inhibition with voltage-gated currents of pyramidal cells: computational mechanism of a sensory searchlight. *J. Neurophysiol.* **80,** 3197–3213 (1998).
24. Glass, L. & Mackey, M. C. *From Clocks to Chaos* (Princeton Univ. Press, Princeton, New Jersey, 1988).
25. Doiron, B., Laing, C., Longtin, A. & Maler, L. Ghostbursting: a novel neuronal burst mechanism. *J. Comput. Neurosci.* **12,** 5–25 (2002).
26. Lemon, N. & Turner, R. W. Conditional spike backpropagation generates burst discharge in a sensory neuron. *J. Neurophysiol.* **84,** 1519–1530 (2000).
27. Bastian, J., Chacron, M. J. & Maler, L. Receptive field organization determines pyramidal cell stimulus encoding capability and spatial stimulus selectivity. *J. Neurosci.* **22,** 4577–4590 (2002).
28. Gabbiani, F., Metzner, W., Wessel, R. & Koch, C. From stimulus encoding to feature extraction in weakly electric fish. *Nature* **384,** 564–567 (1996).
29. Contreras, D., Destexhe, A., Sejnowski, T. J. & Steriade, M. Control of spatiotemporal coherence of a thalamic oscillation by corticothalamic feedback. *Science* **274,** 771–774 (1996).
30. Kloeden, P. E. & Platen, E. *Numerical Solutions to Stochastic Differential Equations* (Springer, Berlin, 1992).

Supplementary Information accompanies the paper on *Nature*'s website (http://www.nature.com/nature).

Acknowledgements We thank J. Lewis, C. Laing, R. W. Turner and M. Higley for reading the manuscript. Funding was provided by the National Science and Engineering Research Council (B.D., M.J.C., A.L.), the Canadian Institutes of Health Research (A.L., L.M.) and the National Institutes of Health (J.B.).

Competing interests statement The authors declare that they have no competing financial interests.

Correspondence and requests for materials should be addressed to B.D. (e-mail: bdoiron@science.uottawa.ca).

Fidelity in planar cell polarity signalling

Dali Ma*, Chung-hui Yang†, Helen McNeill‡, Michael A. Simon† & Jeffrey D. Axelrod*

* *Department of Pathology, Stanford University School of Medicine, Stanford, California 94305-5324, USA*
† *Department of Biological Sciences, Stanford University, Stanford, California 94305, USA*
‡ *Cancer Research UK, London Research Institute, 44 Lincoln's Inn Fields, London WC2A 3PX, UK*

The polarity of *Drosophila* wing hairs displays remarkable fidelity. Each of the approximately 30,000 wing epithelial cells constructs an actin-rich prehair that protrudes from its distal vertex and points distally. The distal location and orientation of the hairs is virtually error free, thus forming a nearly perfect parallel array. This process is controlled by the planar cell polarity signalling pathway[1–4]. Here we show that interaction between two tiers of the planar cell polarity signalling mechanism results in the observed high fidelity. The first tier, mediated by the cadherin Fat[5], dictates global orientation by transducing a directional signal to individual cells. The second tier, orchestrated by the 7-pass transmembrane receptor Frizzled[6,7], aligns each cell's polarity with that of its neighbours through the action of an intercellular feedback loop, enabling polarity to propagate from cell to cell[8]. We show that all cells need not respond correctly to the presumably subtle signal transmitted by Fat. Subsequent action of the Frizzled feedback loop is sufficient to align all the cells cooperatively. This economical system is therefore highly robust, and produces virtually error-free arrays.

A group of signalling molecules, including Frizzled (Fz)[7], Dishevelled (Dsh)[9], Flamingo (Fmi)[10,11], Van Gogh[12,13] and Prickle (Pk)[14] mediates planar cell polarity (PCP) signalling in various developing *Drosophila* tissues[1–4]. In wing cells, these proteins participate in an intercellular feedback loop that generates subcellular asymmetry and directs prehair location[8,15,16]. Frizzled on the distal side of one cell recruits Dsh to the membrane, thus stabilizing Fz localization, and simultaneously recruits Pk to the proximal side of the adjacent cell, where it prevents Dsh localization (Fig. 1a). A competition therefore occurs between Fz on either side of the intercellular boundary, amplifying small differences in Fz levels to all-or-none differences[8]. Coupled with the observation that cells do not accumulate high Fz levels and construct prehairs on two sides, this mechanism enables polarity to propagate from cell to cell (Fig. 1b). For example, removing Fz from a clone of cells produces a difference in Fz at the distal boundary of the clone that is reversed from the wild type, and this reversal propagates, resulting in the 'domineering non-autonomy' first described by ref. 6 (Fig. 1b). The question remains, however, of what initiates the imbalance of Fz activity along the proximal–distal axis of each cell in a wild-type wing. We have proposed previously that, in the eye, two